

Joint Path Selection and Rate Allocation Framework for 5G Self-Backhauled mmWave Networks

Trung Kien Vu, *Student Member, IEEE*, Mehdi Bennis, *Senior Member, IEEE*,
Mérrouane Debbah, *Fellow, IEEE*, and Matti Latva-aho, *Senior Member, IEEE*

Abstract—Owing to severe path loss and unreliable transmission over a long distance at higher frequency bands, we investigate the problem of path selection and rate allocation for multi-hop self-backhaul millimeter wave (mmWave) networks. Enabling multi-hop mmWave transmissions raises a potential issue of increased latency, and thus, in this work we aim at addressing the fundamental questions: “*how to select the best multi-hop paths and how to allocate rates over these paths subject to latency constraints?*”. In this regard, we propose a new system design, which exploits multiple antenna diversity, mmWave bandwidth, and traffic splitting techniques to improve the downlink transmission. The studied problem is cast as a network utility maximization, subject to an upper delay bound constraint, network stability, and network dynamics. By leveraging stochastic optimization, the problem is decoupled into: (i) path selection and (ii) rate allocation sub-problems, whereby a framework which selects the best paths is proposed using reinforcement learning techniques. Moreover, the rate allocation is a non-convex program, which is converted into a convex one by using the successive convex approximation method. Via mathematical analysis, we provide a comprehensive performance analysis and convergence proofs for the proposed solution. Numerical results show that our approach ensures reliable communication with a guaranteed probability of up to 99.9999%, and reduces latency by 50.64% and 92.9% as compared to *baseline models*. Furthermore, the results showcase the key trade-off between latency and network arrival rate.

Keywords—*Low latency and reliable communication (URLLC), self-backhaul, mmWave communications, multi-hop scheduling, ultra-dense small cells, stochastic optimization, reinforcement learning.*

I. INTRODUCTION

The fifth generation (5G) wireless systems are expected to support high data rates of multiple gigabits per second (Gbps) and to have 50 billion connected devices by the year 2020 [2]. In this regard, both academia and industry have paid attention to the underutilized frequency bands (30 – 300 GHz) due to the current scarcity of wireless spectrum [2], [3],

[4]. Moreover, the required capacity demand can be achieved by; (i) advanced spectral-efficient techniques, e.g., massive multiple-input multiple-output (MIMO); and (ii) ultra-dense self-backhauled small cell (SC) deployments [4], [5], [6]. Indeed, massive MIMO has been recognized as one of the promising 5G techniques, which yields remarkable properties such as high signal-to-interference-plus-noise ratio (SINR) due to extreme spatial multiplexing gain [7]. The basic concept of massive MIMO is to utilize hundreds or thousands of antennas at the macro base station (BS) to serve up to tens or hundreds of user equipments (UEs) [6]. More importantly, ultra dense SC deployment provides an effective solution to increase network capacity and coverage [4], [8], [9], in which recent advances in full-duplex (FD) potentially doubles spectral efficiency and reduces latency. In addition to the huge capacity demand, the issues of latency and reliability represent concerns in 5G networks and beyond [2], [10], [11], [12].

In this paper, we investigate the above 5G techniques, namely mmWave communication, massive MIMO, and ultra-dense SC deployment, envisaged as the key enablers for providing great enhancements in terms of high data rate, low latency, and ultra reliable communication [2], [4]. In particular, an in-band wireless backhauling enables such ultra-dense SC deployment [5], [6], [13], [14] when massive MIMO and mmWave are combined to provide Gigabits capacity for wireless backhaul [7], [15]. Although mmWave frequency bands offer huge bandwidth, operating at higher frequency bands experiences high propagation attenuation [3], which requires smart beamforming to achieve highly directional gain [15]. Owing to the short wavelength, mmWave frequency bands allow for packing a massive number of antennas into highly directional beamforming over a short distance. Besides that, transmitting over a long distance, mmWave communication requires higher transmit power and is very sensitive to blockage [3], [6], [4]. Hence, instead of using a single hop [6], [10], a multi-hop self-backhauling architecture is a promising solution to enable transmissions over long distances in 5G mmWave networks [16], [17]. The authors in [18] studied the multi-hop routing for device-to-device mmWave communication, focusing on maximizing the quality of multimedia applications. Further, using multi-hop transmissions raises the potential issue of increased delay, which has been generally ignored [17], [19], [18], [20], [21], [22]. More importantly, the ultra-dense SC network is mainly operated based on the multi-hop multi-path transmission [4], [8], [16]. Hence, there is a need for fast and efficient multi-hop scheduling with respect to traffic dynamics and channel variances in 5G self-backhauled

This research has been financially supported by the Academy of Finland 6Genesis Flagship (grant 318927). The Academy of Finland funding via the grant 307492 and the CARMA grants 294128 and 289611, and the Nokia Foundation are also acknowledged.

T. K. Vu, M. Bennis, and M. Latva-aho are with the Centre for Wireless Communications, University of Oulu, 90014 Oulu, Finland, (email: {trungkien.vu, mehdi.bennis, matti.latva-aho}@oulu.fi).

M. Debbah is with the Large Networks and System Group (LANEAS), CentraleSupélec, Université Paris-Saclay, 91192 Gif-sur-Yvette, France, and also with the Mathematical and Algorithmic Sciences Laboratory, Huawei France R&D, 92100 Paris, France (e-mail: merouane.debbah@huawei.com).

This paper was presented in part at the IEEE WCNC 2018 conference in Barcelona, Catalonia, Spain, April, 2018 [1].

mmWave networks [16], [23]. These previous works have not studied the problem of joint path selection and rate allocation optimization in mmWave networks to ensure Gbps data rate and low latency with reliable communications. To the best of our knowledge, we are perhaps the first to provide a theoretical and practical framework for addressing the above concerns.

A. Main contributions

Considering a multi-hop self-backhauled mmWave network, we propose a new system design to support ultra-reliable and low latency communication (URLLC) with multiple Gbps data rates in which the main contributions of our work are listed as follows:

- A joint path selection and rate allocation optimization for multi-hop multi-path scheduling, whereby self-backhauled FD SCs act as relay nodes to forward data from the macro BS to the intended UEs, is modeled. MmWave communication over a long distance faces the problem of high path loss and blockage. To overcome this challenge, we first combine massive MIMO and mmWave communication techniques to enhance the downlink transmission. Then we propose a latency and reliability aware multi-hop scheduling scheme incorporating a traffic splitting technique to provide Gigabits wireless data rate with URLLC. For this purpose, the studied problem is cast as a network utility maximization (NUM), subject to a bounded delay constraint with a guaranteed probability and network stability.
- Leveraging stochastic optimization framework [24], we decouple the studied problem into two sub-problems, namely path selection and rate allocation. By utilizing the benefits of historical information, we first propose a reinforcement learning-based path selection algorithm to build an empirical distribution of the system dynamics to aid in learning to select the best paths. Therein, the concept of regret strategy is employed, defined as the difference between the average utility when choosing the same paths in previous times, and its average utility obtained by constantly selecting different paths. The premise is that regret is minimized over time so as to choose the best paths. Second, the rate allocation sub-problem is a non-convex combinatorial program, and hence by exploiting the hidden convexity of the problem, we propose an iterative rate allocation algorithm based on the second-order cone program (SOCP) to obtain a local optimal of the approximated convex problem.
- The proposed approach answers the following fundamental questions: *(i) over which paths the traffic flow should be forwarded?* and *(ii) what is the data rate per flow/sub-flow?*, while ensuring a probabilistic delay constraint, and network stability. By using a mathematical analysis, a comprehensive performance of our proposed stochastic optimization framework is scrutinized. It is shown that there exists an $[\mathcal{O}(1/\nu), \mathcal{O}(\nu)]$ utility-queue backlog trade-off, which leads to an utility-delay balancing [24], where ν is a control parameter. In addition, a

convergence analysis of both two sub-problems is studied. Finally, the performance of the proposed solution is validated by extensive set of simulations.

B. Related work

Recently, a performance analysis of multi-hop scheduling for mmWave network was studied in [25]. This paper considered the problem of joint scheduling and congestion control in a multi-hop mmWave network using a NUM framework, without considering key aspects such as the best paths selection, and low latency requirements. Authors in [17] proposed cross-layer modeling to enable multiGigabit for indoor wireless personal area networks by using multi-hop relays and highly directional beamforming in maintaining consistently high throughput. A large body of research work has attempted to study the joint rate allocation, congestion control, routing, and scheduling for multi-hop wireless networks, incorporating the proportional delay based on the sum of queue backlogs [19], applying the concept of back-pressure algorithm [26], [27], or exploiting the potential of multiple gateways [20]. However, other important aspects in 5G networks such as low latency and reliability are generally ignored when maximizing the network performance (capacity, energy efficiency and spectral efficiency) [28], [29].

A recent work in [21] has studied the multi-hop relaying transmission challenges for mmWave systems, aiming at maximizing overall network throughput, and taking account of traffic dynamics and link qualities. In our work, we also study the NUM optimization problem, while considering channel variations and network dynamics. Another recent work in [30] has addressed the problem of traffic allocation for multi-hop scheduling in mmWave networks to minimize the end-to-end latency, in which the minimum latency is derived based on the channel capacity to determine the portions of traffic over channels such that all traffic fractions arrive simultaneously at the destination. In addition, the problem of path selection and multi-path congestion control for data transfers was studied in [22] in which the aggregate utility is increased as more paths are provided. However, splitting data into too many paths leads to increased signaling overhead and causes traffic congestion. While interesting, the preceding works do not address the problem of high-data rate, low-latency and reliability communication in multi-path networks. In this respect, our proposed solution is to select the best paths to maximize the network throughput, subject to a delay bound violation constraint with a tolerable probability (reliability). In particular, we answer the two fundamental questions: *(i)* how to select the best paths while taking traffic dynamics and link qualities into account and *(ii)* how to capture the URLLC while maximizing the network utility in multi-hop self-backhauled mmWave networks. Our previous work [10] studied URLLC-centric mmWave networks for single hop transmission, and hence in this work we extend it to the multi-hop wireless backhaul scenario, and study a joint path selection and rate allocation problem. Via mathematical analyses and extensive simulations, we provide insights into the performance analysis of our proposed algorithm and the convergence characteristics of the learning algorithm and the SOCP based iterative method.

The rest of the paper is organized as follows. Section II describes the system model and Section III provides the problem formulation for a joint path selection and rate allocation optimization. Section IV introduces a stochastic optimization framework to decouple our studied problem, whereby two practical solutions are proposed. A mathematical analysis of the proposed framework is discussed in Section V. In Section VI, we provide extensive numerical results to compare again other baselines. Conclusions are drawn in Section VII.

Notations: Throughout the paper, the lowercase letters, boldface lowercase letters, (boldface) uppercase letters and italic boldface uppercase letters are used to represent scalars, vectors, matrices, and sets, respectively. \mathbf{X}^\dagger and $\text{rank}(\mathbf{X})$ denote the Hermitian transpose and the rank of matrix \mathbf{X} , respectively. $\mathbb{E}[\cdot]$ denotes the expectation operator, $\mathbb{I}_{\{z\}}$ is the indicator function for logic z , and $[x]^+ \triangleq \max\{x, 0\}$. The cardinality of a set \mathcal{S} , is denoted by $|\mathcal{S}|$. We denote the previous hop and the next hop from node i as $i^{(1)}$ and $i^{(o)}$, respectively. $\text{Pr}(\cdot)$ denotes the probability operator.

II. SYSTEM MODEL

A. Network Model

Let us consider a downlink (DL) transmission of a multi-hop heterogeneous cellular network (HCN) which consists of a macro base station (MBS), a set of B self-backhauled small cell base stations (SCBSs), and a set \mathcal{K} of K single-antenna user equipments (UEs) as shown in Fig 1. Let $\mathcal{B} = \{0, 1, \dots, B\}$ denote the set of all BSs in which index 0 refers to the MBS. The in-band wireless backhaul is used to provide backhaul among BSs [13], [31]. A full-duplex (FD) transmission protocol is assumed at SCBS with perfect self-interference cancellation (SIC) capabilities [32]. Each BS is equipped with N_b transmitting antennas and we denote the propagation channel between BS b and UE k as $\mathbf{h}_{(b,k)} = \sqrt{N_b} \Theta_{(b,k)}^{1/2} \mathbf{w}_{(b,k)}$ [6], where $\Theta_{(b,k)} \in \mathbb{C}^{N_b \times N_b}$ depicts the antenna spatial correlation, and the elements of $\mathbf{w}_{(b,k)} \in \mathbb{C}^{N_b \times 1}$ are independent and identically distributed (i.i.d.) with zero mean and variance $1/N_b$.

The network topology is modeled as a directed graph $\mathcal{G} = (\mathcal{N}, \mathcal{L})$, where $\mathcal{N} = \mathcal{B} \cup \mathcal{K}$ represents the set of nodes including BSs and UEs. $\mathcal{L} = \{(i, j) | i \in \mathcal{B}, j \in \mathcal{N}\}$ denotes the set of all directional edges (i, j) in which nodes i and j are the transmitter and the receiver, respectively.

We consider a queuing network operating in discrete time $t \in \mathbb{Z}^+$. There are F independent data flows at the MBS. Each data traffic is destined for only one UE, whereas one UE can receive multiple data streams, i.e., $F \geq K$. Hereafter, we refer to data traffic as data flow. We use $\overline{\mathcal{F}}$ to represent the set of F data flows/sub-flows. The MBS can split each flow $f \in \overline{\mathcal{F}}$ into multiple sub-flows which are delivered via disjoint paths and aggregated at UEs [33].

We assume that there exists Z_f number of disjoint paths from the MBS to the UE for flow f . For any disjoint path $m \in \{1, \dots, Z_f\}$, we denote \mathcal{Z}_f^m as the path state, which contains all path information such as topology and queue states for every hop. Let $\mathcal{Z}_f = \{\mathcal{Z}_f^1, \dots, \mathcal{Z}_f^m, \dots, \mathcal{Z}_f^{Z_f}\}$ denote the path states/tables observed by flow f . We use the flow-split

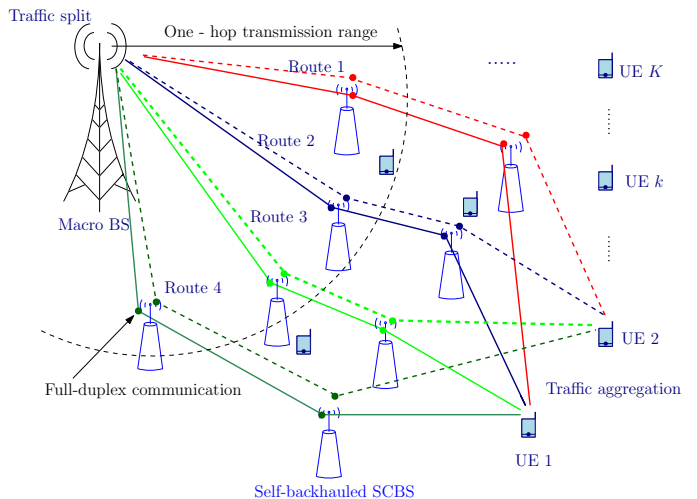


Fig. 1. Illustration of 5G multi-hop self-backhauled mmWave networks.

indicator vector $\mathbf{z}_f = (z_f^1, \dots, z_f^{Z_f})$ to denote how the MBS splits flow f , where $z_f^m = 1$ means path m is used to send data for flow f ; otherwise, $z_f^m = 0$. Let $\mathcal{N}_i^{(o)}$ denote the set of next hops from node i via a directional edge. We denote the next hop and the previous hop of flow f from and to BS i as $i_f^{(o)}$ and $i_f^{(1)}$, respectively. Table I shows the notations, used throughout this paper.

B. Rate Formulation

The channel propagation vector is denoted as $\mathbf{h} = (\mathbf{h}_{(i,j)} | (i, j) \in \mathcal{L})$, and we denote $p_{(i,j)}^f$ as the transmit power of node i assigned to node j for flow f , such that $\sum_{f \in \overline{\mathcal{F}}} \sum_{j \in \mathcal{N}_i^{(o)}} p_{(i,j)}^f \leq P_i^{\max}$, where P_i^{\max} is the maximum transmit power of node i . We have the following power constraint

$$\mathcal{P} = \left\{ p_{(i,j)}^f \geq 0, i, j \in \mathcal{N}, \left| \sum_{f \in \overline{\mathcal{F}}} \sum_{j \in \mathcal{N}_i^{(o)}} p_{(i,j)}^f \leq P_i^{\max} \right. \right\}. \quad (1)$$

Vector $\mathbf{p} = (p_{(i,j)}^f | \forall i, j \in \mathcal{N}, \forall f \in \overline{\mathcal{F}})$ denotes the transmit power over all flows.

Here, we assume that each BS adopts the hybrid beamforming architecture, which enjoys both analog and digital beamforming techniques [34]. For the analog beamforming, let $g_{(i,j)}^{(t)}$ and $g_{(i,j)}^{(r)}$ denote the transmitter and receiver beamforming gain at the transmitter i and the receiver j , respectively. In addition, we use $\omega_{(i,j)}^{(t)}$ and $\omega_{(i,j)}^{(r)}$ to represent the angles deviating from the strongest path between the transmitter i and the receiver j . Also, let $\theta_{(i,j)}^{(t)}$ and $\theta_{(i,j)}^{(r)}$ denote the beamwidth at the transmitter i and the receiver j , respectively. We denote $\boldsymbol{\theta}$ as a vector of the transmitter beamwidth of all BSs. We adapt the widely used antenna radiation pattern model [34], [35], [36] to determine the beamforming gain as

Notations	Descriptions
B, K	Sets of $(B+1)$ base stations, K user equipments
$\mathcal{N} = B \cup K$	Set of nodes including BSs and UEs
\mathcal{L}	Set of all directional edges $(i, j) i \in B, j \in \mathcal{N}$
\mathcal{F}	Set of F flows
\mathcal{Z}_f	Set of Z_f disjoint paths observed by flow f
\mathcal{Z}_f^m	Disjoint path state/table m observed by flow f
$\mathcal{N}_i^{(o)}$	Set of the next hops from node i
$i_f^{(1)}$	Previous hop of flow f to BS i
$i_f^{(o)}$	Next hop of flow f from BS i
$p_{(i,j)}^f$	Transmit power of node i to node j for flow f
$z_f^m = 1$	Path m is used to send data for flow f
π_f^m	Probability of choosing path m for flow f

$$g_{(i,j)}(\omega_{(i,j)}, \theta_{(i,j)}) = \begin{cases} \frac{2\pi - (2\pi - \theta_{(i,j)})\eta}{\theta_{(i,j)}}, & \text{if } |\omega_{(i,j)}| \leq \frac{\theta_{(i,j)}}{2}, \\ \Gamma, & \text{otherwise,} \end{cases}$$

where $0 < \Gamma \ll 1$ is the side lobe gain. For the digital beamforming phase, we apply the linear precoding scheme $\mathbf{v}_{(i,j)}$, i.e., for the conjugate precoding, $\mathbf{v}(\mathbf{h}_{(i,j)}) = \hat{\mathbf{h}}_{(i,j)}$. Here, $\hat{\mathbf{h}}_{(i,j)}$ is the estimated channel of $\mathbf{h}_{(i,j)}$, such that

$$\hat{\mathbf{h}}_{(i,j)} = \sqrt{N_i} \Theta_{(i,j)}^{1/2} \left(\sqrt{1 - \tau_j^2} \mathbf{w}_{(i,j)} + \tau_j \hat{\mathbf{w}}_{(i,j)} \right),$$

where $\tau_j \in [0, 1]$ reflects the estimation accuracy for receiver j , if $\tau_j = 0$, the perfect channel state information is assumed at the transmitters [37]. $\hat{\mathbf{w}}_{(i,j)} \in \mathbb{C}^{N_i \times 1}$ is the estimated noise vector, also modeled as a random matrix with zero mean and variance of $\frac{1}{N_j}$ [6]. Based on the hybrid model [34], the ergodic achievable rate¹ at the receiver j from the transmitter i can be calculated as per (2), where $p_{(i,j)}$ and $p_{(i',j)}$ are the transmit power from the transmitter i and i' to the receiver j , respectively, and the thermal noise of receiver j is $\eta_{(i,j)} \sim \mathcal{CN}(0, \sigma_{(i,j)}^2)$. In addition, W denotes the system bandwidth of the mmWave frequency band.

For a given channel state and transmit power, the data rate in edge (i, j) over flow f can be posted as a function of channel state and transmit power, i.e., $R_f^{(i,j)}(\mathbf{h}, \mathbf{p})$, such that $\sum_{f \in \mathcal{F}} R_f^{(i,j)} = R^{(i,j)}$. We denote $\mathbf{R} = (R_f^{(i,j)})_{\forall i, j \in \mathcal{N}, \forall f \in \mathcal{F}}$ as a vector of data rates over all flows.

C. Network Queues

Let $Q_f^i(t)$ denote the queue length at a BS i at time slot t for flow f . The queue length evolution at the MBS $i = 0$ is

$$Q_f^i(t+1) = \left[Q_f^i(t) - \sum_{m=1, i_f^{(o)} \in \mathcal{Z}_f^m}^{Z_f} R_f^{(i, i_f^{(o)})}(t), 0 \right]^+ + \mu^f(t), \quad (3)$$

where $\mu^f(t)$ is the data arrival at the MBS during slot t , which is independent and identical distributed (i.i.d.) over time with a mean value $\bar{\mu}^f$. Due to the disjoint paths, for each flow f the incoming rate from the previous hop $i_f^{(1)}$ at the SCBS i is

either from another SCBS or the MBS, and thus, the queue evolution at the SCBS $i = \{1, \dots, B\}$ is given by

$$Q_f^i(t+1) = \left[Q_f^i(t) - R_f^{(i, i_f^{(o)})}(t), 0 \right]^+ + R_f^{(i_f^{(1)}, i)}(t). \quad (4)$$

Definition 1. For any vector $\mathbf{x}(t) = (x_1(t), \dots, x_K(t))$, let $\bar{\mathbf{x}} = (\bar{x}_1, \dots, \bar{x}_K)$ denote the time average expectation of $\mathbf{x}(t)$, where $\bar{\mathbf{x}} \triangleq \lim_{t \rightarrow \infty} \frac{1}{t} \sum_{\tau=0}^{t-1} \mathbb{E}[\mathbf{x}(\tau)]$.

Definition 2. For any discrete queue $Q(t)$ over time slots $t \in \{0, 1, \dots\}$ and $Q(t) \in \mathbb{R}_+$,

- $Q(t)$ is strongly stable if $\lim_{t \rightarrow \infty} \sup \frac{1}{t} \sum_{\tau=0}^{t-1} \mathbb{E}[|Q(\tau)|] < \infty$.
- $Q(t)$ is mean rate stable if $\lim_{t \rightarrow \infty} \frac{\mathbb{E}[|Q(t)|]}{t} = 0$.

A queuing network is stable if each queue is stable.

III. PROBLEM FORMULATION

Assume that the MBS determines which paths to split data flow f with a given probability distribution, i.e., $\boldsymbol{\pi}_f = (\pi_f^1, \dots, \pi_f^{Z_f})$, where for each $m \in \mathcal{Z}_f$ we have $\pi_f^m = \Pr(z_f = z_f^m)$. Here, $\boldsymbol{\pi}_f$ is the probability mass function (PMF) of the flow-split vector, i.e., $\sum_{m=1}^{Z_f} \Pr(z_f^m) = 1$. We denote $\boldsymbol{\pi} = \{\boldsymbol{\pi}_1, \dots, \boldsymbol{\pi}_f, \dots, \boldsymbol{\pi}_F\} \in \Pi$ as the global probability distribution of all flow-split vectors in which Π is the set of all possible global PMFs. Let \bar{x}_f denote the achievable average rate of flow f such that

$$\bar{x}_f \triangleq \lim_{t \rightarrow \infty} \frac{1}{t} \sum_{\tau=0}^{t-1} x_f(\tau),$$

and

$$x_f(\tau) = \sum_{m=1, i_f^{(o)} \in \mathcal{Z}_f^m}^{Z_f} \mathbb{E}_{\mathbf{h}, \mathbf{p}}[\pi_f^m R_f^{(i, i_f^{(o)})}(\tau)] \Big|_{i=0}.$$

We assume that the achievable rate is bounded, i.e.,

$$0 \leq x_f(t) \leq a_f^{\max}, \quad (5)$$

where a_f^{\max} is the maximum achievable rate of flow f at every time t . Vector $\bar{\mathbf{x}} = (\bar{x}_1, \dots, \bar{x}_F)$ denotes the time average of rates over all flows. Let \mathcal{R} denote the rate region, which is defined as the convex hull of the average rates, i.e., $\bar{\mathbf{x}} \in \mathcal{R}$.

¹Note that we omit the beam search/tracking time, since it can be done fast and is negligible compared to the transmission time [38].

$$R^{(i,j)} = \mathbb{E}_{\mathbf{h}, \mathbf{p}} \left[\mathbf{W} \log \left(1 + \frac{p^{(i,j)} g_{(i,j)}^{(t)} g_{(i,j)}^{(r)} |\mathbf{h}_{(i,j)}^\dagger \mathbf{v}^{(i,j)}|^2}{\sum_{i' \neq i} p^{(i',j)} g_{(i',j)}^{(t)} g_{(i',j)}^{(r)} |\mathbf{h}_{(i',j)}^\dagger \mathbf{v}^{(i',j)}|^2 + \sigma_{(i,j)}^2} \right) \right] \quad (2)$$

We define U_0 as the network utility function, i.e., $U_0(\bar{\mathbf{x}}) = \sum_{f \in \mathcal{F}} U(\bar{x}_f)$ [22], [6]. Here, $U(\cdot)$ is assumed to be a twice differentiable, concave, and increasing L -Lipschitz function for all $\bar{\mathbf{x}} \geq 0$. According to Little's law [39], the average queuing delay is defined as the ratio of the queue length to the average arrival rate. By taking account of the probabilistic delay constraints for each flow/subflow, the network utility maximization (NUM) is formulated as follows

$$\text{OP: } \max_{\pi, \mathbf{x}, \mathbf{p}} U_0(\bar{\mathbf{x}}) \quad (6a)$$

$$\text{subject to } \Pr \left(\frac{Q_f^i(t)}{\bar{\mu}_f} \geq \beta \right) \leq \epsilon, \forall t, f \in \mathcal{F}, i \in \mathcal{B}, \quad (6b)$$

$$\lim_{t \rightarrow \infty} \frac{\mathbb{E}[|Q_f^i|]}{t} = 0, \forall f \in \mathcal{F}, \forall i \in \mathcal{B}, \quad (6c)$$

$$\mathbf{x}(t) \in \mathcal{R}, \quad (6d)$$

$$\pi \in \Pi, \quad (6e)$$

and (1), (5),

where β reflects the delay threshold required for UEs, and $\epsilon \ll 1$ is the target probability for reliable communication. The probabilistic delay constraint (6b) implies that the probability that the delay for each flow at node i is greater than β is very small, which captures the constraints of ultra-low latency and reliable communication [10], [40]. It is also used to avoid congestion for each flow f at any point (BS) in the network, since the queue length is ensured less than $\beta \bar{\mu}_f$ with probability $1 - \epsilon$. Hence, (6b) forces the transmission of all BSs without building large queues, and (6c) maintains network stability.

The above problem has a non-linear probabilistic constraint (6b), which cannot be solved directly. Hence, we replace the non-linear constraint (6b) with a linear deterministic equivalent by applying Markov's inequality [41], [10] such that $\Pr(X \geq a) \leq \mathbb{E}[X]/a$ for a non-negative random variable X and $a > 0$. Thus, we relax (6b) as

$$\mathbb{E}[Q_f^i(t)] \leq \bar{\mu}_f \epsilon \beta. \quad (7)$$

Assuming that $\mu^f(t)$ follows a Poisson arrival process [41], we derive the expected queue length in (3) for $i = 0$ as

$$\mathbb{E}[Q_f^i(t)] = t \bar{\mu}_f - \sum_{\tau=1}^t \sum_{m=1, i_f^{(o)} \in \mathcal{Z}_f^m} \pi_f^m R_f^{(i, i_f^{(o)})}(\tau), \quad (8)$$

and the expected queue length in (4), for each SCBS, i.e.,

$$\mathbb{E}[Q_f^i(t)] = \sum_{\tau=1}^t \sum_m \pi_f^m \left(R_f^{(i_f^{(1)}, i)}(\tau) - R_f^{(i, i_f^{(o)})}(\tau) \right). \quad (9)$$

Subsequently, combining the constraints (7) and (8), we obtain, for MBS $i = 0$,

$$\begin{aligned} \bar{\mu}_f(t - \epsilon\beta) - \sum_{\tau=1}^{t-1} \sum_{m=1, i_f^{(o)} \in \mathcal{Z}_f^m} \pi_f^m R_f^{(i, i_f^{(o)})}(\tau) \\ \leq \sum_{m=1, i_f^{(o)} \in \mathcal{Z}_f^m} \pi_f^m R_f^{(i, i_f^{(o)})}(t). \end{aligned} \quad (10)$$

Similarly, for each SCBS $i = \{1, \dots, B\}$, we have

$$\begin{aligned} -\bar{\mu}_f \epsilon\beta + \sum_{\tau=1}^{t-1} \sum_m \pi_f^m \left(R_f^{(i_f^{(1)}, i)}(\tau) - R_f^{(i, i_f^{(o)})}(\tau) \right) \\ \leq \sum_m \pi_f^m \left(R_f^{(i, i_f^{(o)})}(t) - R_f^{(i_f^{(1)}, i)}(t) \right), \end{aligned} \quad (11)$$

by combining (7) and (9). With the aid of the above derivations, we consider (10) and (11) instead of (6b) in the original problem (6). In practice, the statistical information of all candidate paths to decide $\pi_f, \forall f \in \mathcal{F}$, is not available beforehand, and thus solving (6) is challenging. One solution is that paths are randomly assigned to each flow which does not guarantee optimality, whereas applying an exhaustive search is not practical. Therefore, in this work, we propose a low-complexity approach by invoking tools from Lyapunov stochastic optimization which achieves the optimal performance without requiring the statistical information beforehand.

IV. PROPOSED PATH SELECTION AND RATE ALLOCATION ALGORITHM

In this section, we propose a Lyapunov optimization based framework in order to solve our predefined problem (6) with relaxed latency constraints. To do that, we first introduce a set of auxiliary variables to refine the original problem (6). Next, we convert the constraints into virtual queues and write the conditional Lyapunov drift function. Finally, the solution of the equivalent problem is obtained by minimizing the Lyapunov drift and a penalty from the objective function.

Let us start by rewriting (6) equivalently as follows

$$\text{RP: } \max_{\varphi, \pi, \mathbf{p}} U_0(\bar{\varphi}) \quad (12a)$$

$$\text{subject to } \bar{\varphi}_f - \bar{x}_f \leq 0, \forall f \in \mathcal{F}, \quad (12b)$$

$$(1), (5), (6c), (6e), (10), (11),$$

where the new constraint (12b) is introduced to replace the rate constraint (6d) with new auxiliary variables $\varphi = (\varphi_1, \dots, \varphi_F)$. In (12b), $\bar{\varphi} \triangleq \lim_{t \rightarrow \infty} \frac{1}{t} \sum_{\tau=0}^{t-1} \mathbb{E}[|\varphi(\tau)|]$. In order to ensure the inequality constraint (12b), we introduce a virtual queue vector $Y_f(t)$, which is given by

$$Y_f(t+1) = [Y_f(t) + \varphi_f(t) - x_f(t)]^+, \forall f \in \mathcal{F}. \quad (13)$$

Let $\Sigma(t) = (\mathbf{Q}(t), \mathbf{Y}(t))$ denote the queue backlogs. We first write the conditional Lyapunov drift for slot t as

$$\Delta(\Sigma(t)) = \mathbb{E}[L(\Sigma(t+1)) - L(\Sigma(t)) | \Sigma(t)], \quad (14)$$

where $L(\Sigma(t)) \triangleq \frac{1}{2} \left[\sum_{f=1}^F \sum_{i=0}^B Q_f^i(t)^2 + \sum_{f=1}^F Y_f(t)^2 \right]$ is the quadratic Lyapunov function of $\Sigma(t)$ [24]. We then apply the Lyapunov drift-plus-penalty technique [24], [42], [6], where the solution of (12) is obtained by minimizing the Lyapunov drift and a penalty from the objective function, i.e.,

$$\min \quad \Delta(\Sigma(t)) - \nu \mathbb{E}[U_0(\bar{\varphi}) | \Sigma(t)]. \quad (15)$$

Here, ν is a control parameter to trade off utility optimality and queue length [6]. Note that the stability of $\Sigma(t)$ ensures that the constraints of problem (6c) and (12b) are held. Subsequently, following the straightforward calculations of the Lyapunov optimization which are omitted here for space [24], choosing that $\varphi \in \mathcal{R}$ and a feasible π and all possible $\Sigma(t)$ for all t , we obtain

$$(15) \leq \sum_{f=1}^F \sum_{i=1}^B Q_f^i \mathbb{E} \left[\sum_m \pi_f^m \left(R_f^{(i_f^{(1)}, i)} - R_f^{(i_f^{(0)}, i)} \right) | \Sigma(t) \right] \\ - \sum_{f=1}^F Q_f^{i=0} \mathbb{E} \left[\sum_{m=1, i_f^{(0)} \in \mathcal{Z}_f^m} \pi_f^m R_f^{(i_f^{(0)}, i)} | \Sigma(t) \right] \\ + \sum_{f=1}^F \mathbb{E} [Y_f \varphi_f - \nu U(\varphi_f) - Y_f x_f | \Sigma(t)] + \Psi. \quad (16)$$

Here, the constant value Ψ does not influence the system performance [24], [6]. The solution to (12) can be obtained by minimizing the upper bound in (16). For every slot t , observing $\Sigma(t)$, we have three decoupled subproblems and provide the solutions for each subproblem as follows:

The flow-split vector and the probability distribution are determined by

$$\text{SP1: } \min_{\pi} \quad \sum_{f=1}^F \Xi_f \\ \text{subject to} \quad (6e),$$

where

$$\Xi_f = \sum_{i=1}^B Q_f^i \sum_m \pi_f^m \left(R_f^{(i_f^{(1)}, i)} - R_f^{(i_f^{(0)}, i)} \right) \\ - Q_f^{i=0} \sum_{m=1, i_f^{(0)} \in \mathcal{Z}_f^m} \pi_f^m R_f^{(i_f^{(0)}, i)}.$$

Then, we select the optimal auxiliary variables by solving the following convex optimization problem

$$\text{SP2: } \min_{\varphi | \pi} \quad \sum_{f=1}^F [Y_f \varphi_f - \nu U(\varphi_f)] \\ \text{subject to} \quad \varphi_f(t) \geq 0, \forall f \in \mathcal{F}.$$

Let φ_f^* be the optimal solution obtained by the first order derivative of the objective function of SP2. Assuming a logarithmic utility function, we have $\varphi_f^*(t) = \max \left\{ \frac{\nu}{Y_f}, 0 \right\}$. Finally, the rate allocation is done by assigning transmit power, which is obtained by

$$\text{SP3: } \min_{\mathbf{x}, \mathbf{p} | \pi} \quad \sum_{f=1}^F -Y_f x_f \\ \text{subject to} \quad (1), (5), (10), (11).$$

A. Path Selection

Now we leverage regret learning which exploits the historical system information such as queue state and channel state to select the optimal paths in SP1 [43], [29], [12]. The intuition behind this approach is that the regret learning method results in maximizing the long-term utility for each flow. Moreover, the previous work [17], [19], [25], [18] heavily rely on the statistical information to find the solutions, and ignore the potential benefits of historical system information, which can be used to build an empirical distribution of network system to learn the network parameters. Recall that \mathbf{z}_f represents the flow-split vector given to flow f and $z_f^m = 1$ when path m is used to send data for flow f . The MBS selects paths for each flow with a given probability (mixed strategy). The optimal strategies mean that the MBS does not wish to change its strategy for any flow where any deviation does not offer better utility gain for all flows. We denote $u_f^m = u_f(z_f^m, \mathbf{z}_f^{-m})$ as a utility function of flow f when using path m . The vector \mathbf{z}_f^{-m} denotes the flow-split vector excluding path m . The MBS can choose more than one path to deliver data, from SP1, the utility gain of flow f is

$$u_f = \sum_m u_f^m = -\Xi_f.$$

To exploit the historical information, the MBS determines a flow-split vector for each flow f from \mathcal{Z}_f based on the PMF from the previous stage $t-1$, i.e.,

$$\pi_f(t-1) = \left(\pi_f^1(t-1), \dots, \pi_f^{Z_f}(t-1) \right). \quad (17)$$

Here, we define $\mathbf{r}_f(t) = (r_f^1(t), \dots, r_f^m(t) \dots, r_f^{Z_f}(t))$ as a regret vector of determining flow-split vector for flow f . The MBS selects the flow-split vector with highest regret in which the mixed-strategy probability is given as

$$\pi_f^m(t) = \frac{[r_f^m(t)]^+}{\sum_{m' \in \mathcal{Z}_f} [r_f^{m'}(t)]^+}. \quad (18)$$

Let $\hat{\mathbf{r}}_f(t) = (\hat{r}_f^1(t), \dots, \hat{r}_f^m(t) \dots, \hat{r}_f^{Z_f}(t))$ be the estimated regret vector of flow f , we introduce the Boltzmann-Gibbs

(BG) distribution, $\beta_f^m(\hat{\mathbf{r}}_f(t))$ to capture the exploitation and exploration for efficient learning, given by

$$\beta_f^m(\hat{\mathbf{r}}_f(t)) = \operatorname{argmax}_{\pi_f \in \Pi} \sum_{m \in \mathcal{Z}_f} [\pi_f^m(t) \hat{r}_f^m(t) - \kappa_f \pi_f^m(t) \ln(\pi_f^m(t))], \quad (19)$$

where the trade-off factor κ_f is used to balance between exploration and exploitation [44], [43], [29]. If κ_f is small, the MBS selects \mathbf{z}_f with highest payoff. For $\kappa_f \rightarrow \infty$ all decisions have equal probability.

For a given set of $\hat{\mathbf{r}}_f(t)$ and κ_f , we solve (19) to find the probability distribution in which the solution determining the disjoint paths for each flow f is given as

$$\beta_f^m(\hat{\mathbf{r}}_f(t)) = \frac{\exp\left(\frac{1}{\kappa_f} [\hat{r}_f^m(t)]^+\right)}{\sum_{m' \in \mathcal{Z}_f} \exp\left(\frac{1}{\kappa_f} [\hat{r}_f^{m'}(t)]^+\right)}. \quad (20)$$

We denote $\hat{u}(t)$ as the estimated utility of flow f at time instant t with action \mathbf{z}_f , i.e., $\hat{\mathbf{u}}_f(t) = (\hat{u}_f^1(t), \dots, \hat{u}_f^m(t), \dots, \hat{u}_f^{Z_f}(t))$. Upon receiving the feedback, $\tilde{u}_f(t)$ denotes the utility observed by flow f , i.e., $\tilde{u}_f(t) = u_f(t-1)$, we propose the learning mechanism at each time instant t as follows.

Learning procedure: The estimates of the utility, regret, and probability distribution functions are performed, and are updated for all actions per path m as follows:

$$\begin{cases} \hat{u}_f^m(t) = \hat{u}_f^m(t-1) + \xi_f(t) \mathbb{I}_{\{\mathbf{z}_f = \mathbf{z}_f^m\}} (\tilde{u}_f(t) - \hat{u}_f^m(t-1)) \\ \hat{r}_f^m(t) = \hat{r}_f^m(t-1) + \gamma_f(t) (\hat{u}_f^m(t) - \tilde{u}_f(t) - \hat{r}_f^m(t-1)), \\ \pi_f^m(t) = \pi_f^m(t-1) + \iota_f(t) (\beta_f^m(\hat{\mathbf{r}}_f(t)) - \pi_f^m(t-1)), \end{cases} \quad (21)$$

Here, $\xi_f(t)$, $\gamma_f(t)$, and $\iota_f(t)$ are the learning rates (please see Section V for more details and convergence proof). Based on the probability distribution as per (21), the MBS determines the flow-split vector for each flow f . Note that the learning-aided path selection is performed in a long-term period to ensure that the paths do not suddenly change such that the SCBSs have sufficient time to deliver traffic from the queues. For instance, at the beginning of the large time scale, the best paths are selected, and will be used for the rest of these large scale time slots as shown in Fig. 2.

B. Rate Allocation

Consider $R_f^{(i,j)} = \log(1 + p_{(i,j)}^f |g_{(i,j)}(\mathbf{h})|^2)$ as the transmission rate, where the effective channel gain² for mmWave channels can be modeled as $|g_{(i,j)}(\mathbf{h})|^2 = \frac{|\tilde{g}_{(i,j)}(\mathbf{h})|^2}{1 + I_{\max}^f}$ [15], [6]. Here, $\tilde{g}_{(i,j)}(\mathbf{h})$ and I_{\max}^f denote the normalized channel gain and the maximum interference, respectively. Denoting the left hand side (LHS) of (10) and (11) as D_i^f for simplicity, the

²The effective channel gain captures the path loss, channel variations, and interference penalty (Here, the impact of interference is considered small due to highly directional beamforming and high pathloss for interfered signals at mmWave frequency band, and thus a multi-hop directional transmission can be operated at dense mmWave networks [15], [25], [5]).

optimal values of flow control \mathbf{x} and transmit power \mathbf{p} in the sub-problem 3 (SP3) are found by minimizing

$$\min_{\mathbf{x}, \mathbf{p} | \pi} \sum_{f=1}^F -Y_f x_f \quad (22a)$$

$$\text{subject to } 1 + p_{(i,i_f^{(o)})}^f |g_{(i,i_f^{(o)})}|^2 \geq e^{x_f}, \forall f \in \mathcal{F}, i = 0, \quad (22b)$$

$$\frac{1 + p_{(i,i_f^{(o)})}^f |g_{(i,i_f^{(o)})}|^2}{1 + p_{(i_f^{(1)},i)}^f |g_{(i_f^{(1)},i)}|^2} \geq e^{D_i^f}, f \in \mathcal{F}, \forall i = 1 : B, \quad (22c)$$

$$\sum_{f \in \mathcal{F}} p_{(i,i_f^{(o)})}^f \leq P_i^{\max}, \forall i \in \mathcal{B}, \forall f \in \mathcal{F}. \quad (22d)$$

Although the constraint (22c) is non-convex, due to the fact that the LHS of (22c) is an affine-over-affine function, which is jointly convex w.r.t the corresponding variables [45], [46]. In this regard, we introduce the slack variable y to (22c) and rewrite it as

$$\frac{2 + p_{(i,i_f^{(o)})}^f |g_{(i,i_f^{(o)})}|^2}{2} \geq \sqrt{y^2 + \left(\frac{p_{(i,i_f^{(o)})}^f |g_{(i,i_f^{(o)})}|^2}{2}\right)^2}, \quad (23)$$

$$\frac{y^2}{1 + p_{(i_f^{(1)},i)}^f |g_{(i_f^{(1)},i)}|^2} \geq e^{D_i^f}. \quad (24)$$

Here, the constraint (23) holds a form of the second-order cone inequalities [45], [47], while the LHS of constraint (24) is a quadratic-over-affine function which is iteratively replaced by the first order to achieve a convex approximation as follows

$$\frac{2yy^{(l)}}{1 + p_{(i_f^{(1)},i)}^{f(l)} |g_{(i_f^{(1)},i)}|^2} - \frac{y^{(l)2} \left(1 + p_{(i_f^{(1)},i)}^f |g_{(i_f^{(1)},i)}|^2\right)}{\left(1 + p_{(i_f^{(1)},i)}^{f(l)} |g_{(i_f^{(1)},i)}|^2\right)^2} \geq e^{D_i^f}. \quad (25)$$

Here, the superscript l denotes the l th iteration. Hence, we iteratively solve the approximated convex problem of (22) as

Algorithm 1 in which the approximated problem³ is given as

$$\begin{aligned} \min_{\mathbf{x}, \mathbf{p} | \pi} \quad & \sum_{f=1}^F -Y_f x_f \quad (26) \\ \text{subject to} \quad & (22d), (5), (22b), (23), (25). \end{aligned}$$

Finally, the information flow diagram of the learning-aided path selection and rate allocation approach is shown in Fig. 2, where the rate allocation is executed in a short-term period. Note that the path selection and rate allocation are both done at

³Note that the problem of finding the global optimality is outside the scope of our study. The effectiveness of SOCP method was verified in the literature and shown to be robust in practical scenarios [45].

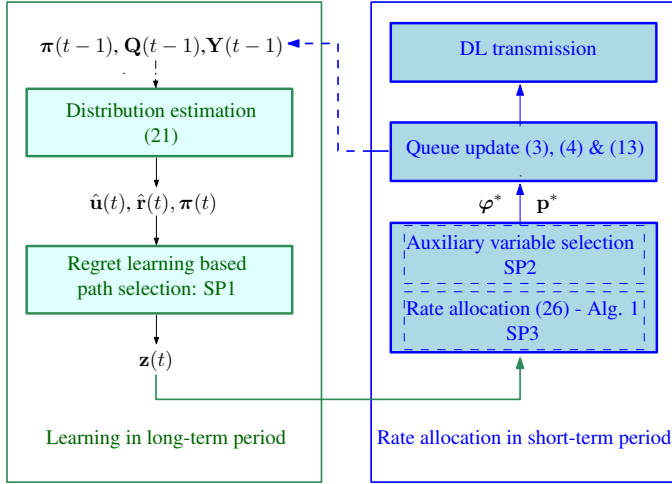


Fig. 2. Information flow diagram of the learning-aided path selection and rate allocation approach.

the MBS, in this work we assume that the information is shared among the base stations by using the X2 interface. As opposed to a brute-force approach yielding the global optimal solution, the proposed iterative solution that uses time scale separation remarkably reduces the search time and computational complexity, while obtaining an efficient suboptimal solution.

Algorithm 1 Iterative rate allocation

Initialization: set $l = 0$ and generate initial points $y^{(l)}$.
repeat
 Solve (26) with $y^{(l)}$ to get the optimal value $y^{(l)*}$.
 Update $y^{(l+1)} := y^{(l)*}$; $l := l + 1$.
until Convergence

V. PERFORMANCE ANALYSIS

In this section, we provide a comprehensive performance analysis of our proposed Lyapunov optimization based framework. We show that there exists an $[\mathcal{O}(1/\nu), \mathcal{O}(\nu)]$ utility-queue backlog trade-off, where ν is the Lyapunov control parameter [24]. Next, we present the conditions that ensure that the proposed learning-based path selection converges with probability one. Finally, a convergence analysis and a complexity computation of the SOCP based approximation method for rate allocation sub-problem are studied.

A. Queue and Utility Performance

We scrutinize the performance analysis of our proposed algorithm and prove that the queues are stable as per the following theorem.

Theorem 3. [Optimality] Assume that all queues are initially empty. For arbitrary arrival rates, the path selection and rate allocation are chosen to satisfy (16) and the rate regime. For a given constant $\chi \geq 0$, the network utility maximization with

any $\nu > 0$ provides the following utility performance with χ -approximation

$$U_0 \geq U_0^* - \frac{\Psi + \chi}{\nu},$$

where U_0^* is the optimal network utility over the rate regime.

Proof: We first prove the queues are bounded. Let \varkappa_f denote the largest right derivative of $U(\bar{x}_f)$, the Lyapunov framework can guarantee the following strong stability of the virtual queues and the network queues.

$$Q_f^i(t) \leq \nu \varkappa_f + a_f^{\max}, \quad (27)$$

$$Y_f(t) \leq \nu \varkappa_f + a_f^{\max}, \quad (28)$$

Here we first prove the bound of the virtual queues, and then the bound of the network queues are proved similarly. Suppose that all queues are initially empty at $t = 1$, this clearly holds for $t = 1$. Suppose these inequalities hold for some $t > 1$, we need to show that it also holds for $t + 1$.

From (13), if $Y_f(t) \leq \nu \varkappa_f$ then $Y_f(t + 1) \leq \nu \varkappa_f + a_f^{\max}$ and the bound holds for $t + 1$ due to the rate constraint $x_f(t) \leq a_f^{\max}$. Else, if $Y_f(t) \geq \nu \varkappa_f$; since the value of auxiliary variables is determined by maximized $\sum_{f=1}^F Y_f(t) \varphi_f(t) - \nu U_0(\varphi(t))$, $\varphi(t)$ is then forced to be zero. From (13), $Y_f(t + 1)$ is bounded by $Y_f(t)$. Since the virtual queues are bounded for t , we have the following inequalities

$$Y_f(t + 1) \leq Y_f(t) \leq \nu \varkappa_f + a_f^{\max}, \quad (29)$$

Hence, the bounds of the virtual queues hold for all t . Similarly, we can prove that the network queue (27) is stable with network queues in (3) and (4).

We have established the network bounds, we are now going to show the utility bound. Since our solution of (6) is to minimize the Lyapunov drift and the objective function every time slot t , we have the following inequality given all existing $\Sigma(t)$ for all t ,

$$\begin{aligned} \Delta(\Sigma(t)) - \nu \mathbb{E}[U_0(\bar{\varphi}(t)) | \Sigma(t)] &\leq \\ &\sum_{f=1}^F \sum_{i=1}^B Q_f^i \mathbb{E} \left[\sum_m \pi_f^{m*} \left(R_f^{(i_f^{(1)}, i)} - R_f^{(i, i_f^{(o)})} \right) | \Sigma(t) \right] \\ &- \sum_{f=1}^F Q_f^{i=0} \mathbb{E} \left[\sum_{m=1, i_f^{(o)} \in \mathcal{Z}_f^m} \pi_f^{m*} R_f^{(i, i_f^{(o)})} | \Sigma(t) \right] \\ &+ \sum_{f=1}^F \mathbb{E} [Y_f \varphi_f^* - \nu U(\varphi_f^*) - Y_f x_f^* | \Sigma(t)] + \Psi, \end{aligned}$$

where $\varphi_f^*(t)$, and $x_f^*(t)$ are the optimal values of the sub-problems SP2 and SP3, respectively. Here, π_f^{m*} and z_f^{m*} are the optimal values of the sub-problem SP1. Since the queues are bounded, for a given $\chi \geq 0$, we obtain

$$\Delta(\Sigma(t)) - \nu \mathbb{E}[U_0(\varphi(t)) | \Sigma(t)] \leq \Psi - \nu \mathbb{E}[U_0(\varphi^*(t)) | \Sigma(t)] + \chi.$$

By taking expectations of both sides of the above inequality and choosing $\mathbf{x}^*(t) = \varphi^*(t)$, it yields for all $t \geq 0$,

$$\mathbb{E}[L(\Sigma(t+1)) - L(\Sigma(t)) | \Sigma(t)] - \nu \mathbb{E}[U_0(\varphi(t)) | \Sigma(t)] \leq \Psi + \chi - \nu \mathbb{E}[U_0(\mathbf{x}^*(t))].$$

By taking the sum over $\tau = 1, \dots, t$ and dividing by t , (using the fact that $U_0(\mathbf{x}^*(t)) = U_0^*$), yielding

$$\frac{\mathbb{E}[L(\Sigma(t+1)) - L(\Sigma(0)) | \Sigma(0)]}{t} - \frac{\nu}{t} \sum_{\tau=1}^t \mathbb{E}[U_0(\varphi(\tau)) | \Sigma(\tau)] \leq \Psi + \chi - \nu U_0^*. \quad (30)$$

By using the fact that $L(\Sigma(t+1)) \geq 0$ and $L(\Sigma(\tau=1)) = 0$, and applying Jensen's inequality in the concave function and rearranging the terms yields

$$U_0(\varphi(t)) \geq U_0^* - \frac{\Psi + \chi}{\nu}.$$

Since the network utility function is a non-decreasing concave function, the auxiliary variable is chosen to satisfy $x_f(t) \geq \varphi_f(t)$. Hence $U_0(\mathbf{x}(t)) \geq U_0(\varphi(t)) \geq U_0^* - \frac{\Psi + \chi}{\nu}$, which means that the solution is closed to the optimal as increasing ν . Which completes the proof of the **Theorem 3**. ■

Hence, there exists an $[\mathcal{O}(\nu), \mathcal{O}(1/\nu)]$ utility-queue length trade-off, which leads to an utility-delay balancing. We now prove that all queues are stable, the bound (30) can be rewritten as

$$\Delta(\Sigma(t)) \leq C,$$

where C is any constant that satisfies for all t and $\Sigma(t)$: $C \geq \Psi + \chi - \nu(U_0^* - \mathbb{E}[U_0(\varphi(t)) | \Sigma(t)])$. By using the definition of the Lyapunov drift and taking an expectation, obtaining

$$\mathbb{E}[L(\Sigma(t))] \leq Ct.$$

As the definition of the Lyapunov function $L(\Sigma(t))$, $\forall i \in \mathcal{B}$ we have

$$\mathbb{E}[Q_f^i(t)]^2, \mathbb{E}[Y_f(t)]^2 \leq 2Ct.$$

Dividing both sides by t^2 , and taking the square roots shows for all $t > 0$ and $\forall i \in \mathcal{B}$:

$$\frac{\mathbb{E}[Q_f^i(t)]}{t}, \frac{\mathbb{E}[Y_f(t)]}{t} \leq \sqrt{\frac{2C}{t}}.$$

As $t \rightarrow \infty$, taking the limit, we prove the queues are stable.

B. Learning Convergence Conditions

Here, we briefly establish the convergence conditions to the \circ -coarse correlated equilibrium for the reinforcement learning based algorithm, where \circ is a very small positive value [43]. The complete proof was studied in [43], [29], the learning rates $\xi_f(t)$, $\gamma_f(t)$, and $\iota_f(t)$ are chosen to satisfy the convergence conditions as follows:

$$\begin{cases} \lim_{t \rightarrow \infty} \sum_{\tau=0}^t \xi_f(\tau) = +\infty, & \lim_{t \rightarrow \infty} \sum_{\tau=0}^t \gamma_f(\tau) = +\infty, \\ \lim_{t \rightarrow \infty} \sum_{\tau=0}^t \iota_f(\tau) = +\infty, & \lim_{t \rightarrow \infty} \sum_{\tau=0}^t \xi_f^2(\tau) < +\infty, \\ \lim_{t \rightarrow \infty} \sum_{\tau=0}^t \gamma_f^2(\tau) < +\infty, & \lim_{t \rightarrow \infty} \sum_{\tau=0}^t \iota_f^2(\tau) < +\infty, \\ \lim_{t \rightarrow \infty} \frac{\iota_f(t)}{\gamma_f(t)} = 0, & \lim_{t \rightarrow \infty} \frac{\gamma_f(t)}{\xi_f(t)} = 0. \end{cases}$$

C. Convergence Analysis of SOCP based Algorithm 1

We establish a convergence result for **Algorithm 1** based on the SOCP approach. By using the SOCP approach, we have approximated the original non-convex problem (22) by a strongly convex problem (26). We briefly describe the convergence for the sake of completeness since it was studied in [48]. We assume that the **Algorithm 1** obtains the solution of problem (26) at iteration $l+1$ th. The updating rule in **Algorithm 1** ensures that the optimal values $\mathbf{y}^{(l)}$ at iteration l satisfy all constraints in (26) and are feasible to the optimization problem at iteration $l+1$. Therefore, the objective obtained in the $l+1$ st iteration is less than or equal to that in the l th iteration, since we minimize the linear function. In other words, **Algorithm 1** yields a non-increasing sequence. Due to the transmit power constraints and rate constraints, the objective is bounded, and thus **Algorithm 1** converges to some local optimal solution of (26). Moreover, **Algorithm 1** produces a sequence of points that are feasible for the original problem (22) and this solution satisfies the Karush–Kuhn–Tucker (KKT) condition of the original problem (22) as discussed in [48].

VI. NUMERICAL RESULTS

In this section Monte Carlo simulations are carried out in order to evaluate the system performance of our proposed algorithm. In particular, we provide numerical results by assuming two flows from the MBS to two UEs, while the number of available paths for each flow is four [22]. The MBS selects two paths from four most popular paths⁴. Each path contains two relays, the total number of SCBSs is 8, and the one-hop distance is varying from 50 to 100 meters. The maximum transmit power of MBS and each SC are 43 dBm and 30 dBm, respectively. The SC antenna gain is 5 dBi and the number of antennas at each BS is $N_b = 8$. We assume that the traffic flow is divided equally into two sub-flows, the arrival rate for each sub-flow is varying from 2 to 5 Gbps. The path loss is modeled as a distance-based path loss with the line-of-sight (LOS) model⁵ for urban environments at 28 GHz with a 1 GHz system bandwidth [49]. The maximum delay requirement β and the target reliability probability ϵ are set to be 10 ms and 5%, respectively [10]. For the learning algorithm, the Boltzmann temperature (trade-off factor) κ_f is set to 5, while the learning rates $\xi_f(t)$, $\gamma_f(t)$, and $\iota_f(t)$ are set to $\frac{1}{(t+1)^{0.51}}$, $\frac{1}{(t+1)^{0.55}}$, and $\frac{1}{(t+1)^{0.6}}$, respectively [29], [11]. The parameter settings⁶ are summarized in Table II.

Furthermore, we compare our proposed scheme with the following baselines:

- **Baseline 1** considers a general NUM framework [24], [27] with path learning algorithm [43].

⁴As studied in [22], it suffices for a flow to maintain at least two paths provided that it repeatedly selects new paths at random and replaces if the latter provides higher throughput.

⁵The probability of LOS communication is assumed to be high for one-hop transmission, while the blockage channel is modeled for the baseline with single-hop scheme.

⁶A simulation source code can be found in [50].

Parameter	Values
B, K, F	8, 2, 4
Number of antennas N_b	8
Maximum transmit power of MBS	43 dBm
Maximum transmit power of SCBS	30 dBm
SCBS antenna gain	5dBi
Carrier frequency	28 GHz
System bandwidth W	1 GHz
Maximum delay β	10 ms
Target reliability ϵ	0.05, 0.1, 0.15
Boltzmann temperature	2, 5, 10, 20, 50

- **Baseline 2** considers a general NUM framework [24], [27] and a random path section scheme, subject to (6b).
- **Baseline 3** considers a general NUM framework [24], [27] and a random path section scheme.
- **Single hop** scheme: The MBS delivers data to UEs over one single hop at long distance in which the probability of LOS communication is low, and then the blockage needs to be taken into account [49].

In Fig. 3, we report the average one-hop delay⁷ versus the mean arrival rates $\bar{\mu}$. As we increase $\bar{\mu}$, **baselines 3**, **2**, and **1** violate the latency constraints at $\bar{\mu} = 3.5, 4.5$, and 5 Gbps, respectively. While the average delay of our proposed algorithm is gradually increased with $\bar{\mu}$, but under the warming level, $\beta = 10$ ms. The reason behind this gain is that the delay requirement is satisfied via the equivalent instantaneous rate by our proposed algorithm as per (10) and (11), while the **baselines 1** and **3** use the traditional utility-delay trade-off approach without considering the latency constraint, and the **baseline 2** considers the random path selection mechanism only. The benefit of applying the learning path algorithm is that selecting the path with high payoff and less congestion, results in small latency. Let us now take a look at $\bar{\mu} = 4.5$ Gbps, the average one-hop delay of **baseline 1** with learning outperforms **baselines 2** and **3**, whereas our proposed scheme reduces latency by 50.64%, 81.32% and 92.9% as compared to **baselines 1**, **2**, and **3**, respectively. When $\bar{\mu} = 5$ Gbps, the average delay of all **baselines** increases dramatically, violating the delay requirement of 10 ms, while our proposed scheme is robust to the latency requirement.

In Fig. 4, we report the tail distribution (complementary cumulative distribution function (CCDF)) of latency to showcase how often the system achieves a delay greater than the target delay levels [51]. In contrast to the average delay, the tail distribution is an important metric to reflect the URLLC characteristic. For instance, at $\bar{\mu} = 4.5$ Gbps, by imposing the probabilistic latency constraint, our proposed approach ensures reliable communication with better guaranteed probability, i.e., $\Pr(\text{delay} > 10\text{ms}) < 10^{-6}$. In contrast, **baseline 1** with learning violates the latency constraint with high probability, where $\Pr(\text{delay} > 10\text{ms}) = 0.08$ and $\Pr(\text{delay} > 25\text{ms}) < 10^{-6}$, while the performance of **baselines 2** and **3** gets worse. For instance, as shown in Fig. 4, **baselines 2** and **3** obtain $\Pr(\text{delay} > 10\text{ms}) > 0.12$ and $\Pr(\text{delay} > 10\text{ms}) > 0.24$, respectively. For throughput comparison, we observe that for $\bar{\mu} = 4.5$ Gbps, our proposed algorithm is able to deliver 4.4874 Gbps of average network throughput per each sub-flow, while

⁷The average end-to-end delay is defined as the sum of the average one-hop delay of all hops.

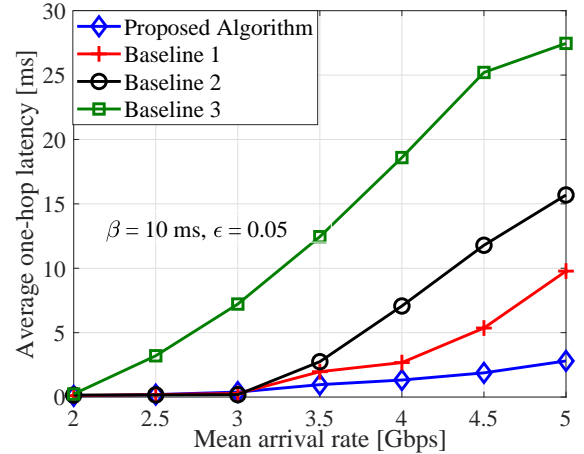


Fig. 3. Average one-hop delay versus mean arrival rates, $\epsilon = 0.05$, $\beta = 10$ ms, $\kappa = 5$.

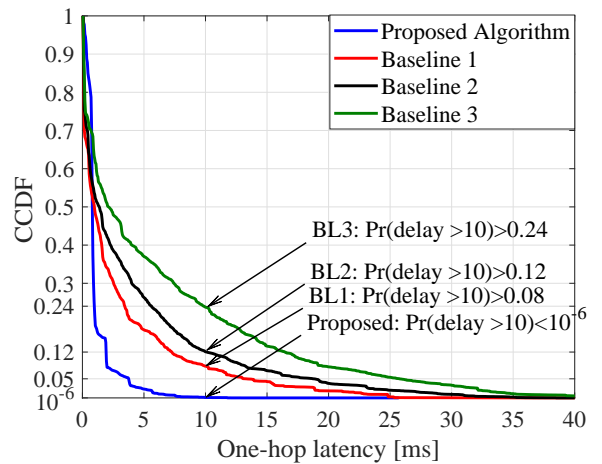


Fig. 4. CCDF of the one-hop latency, $\bar{\mu} = 4.5$ Gbps, $\epsilon = 0.05$, $\beta = 10$ ms, $\kappa = 5$.

the **baselines 1**, **2**, and **3** deliver 4.4759, 4.4682, and 4.3866 Gbps, respectively. Here, the **Single hop** scheme only delivers 3.55 Gbps due to the high path loss, causing large latency.

Note that in this work we mainly focus on the low latency scale, i.e., 1 – 10 ms, the target achievable rate for all schemes is very high and close to each other. Hence, we report the average MBS queue length instead of the average achievable rate. General speaking, as per (3), the average achievable rate can be extracted from the average MBS queue length and the mean arrival rate, i.e., $\bar{x}_f = \bar{\mu}_f - \bar{Q}_f$. In Fig 5, we plot the average queue length of the MBS as a function of mean arrival rates. As we increase the mean arrival rate from 2 to 5 Gbps, the average MBS queue length of our proposed algorithm is increased from 0.01 Gb to 0.04 Gb, which means that the average delay at the MBS is increased from 5 ms to 8 ms, which meet the latency constraint (6b). In contrast, the average queue length of the baselines is increased up to 16 ms, which violates the latency constraint (6b).

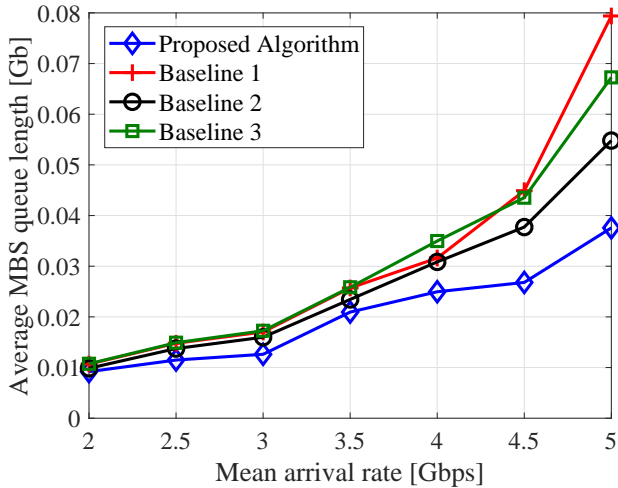


Fig. 5. Average MBS queue length versus mean arrival rate.

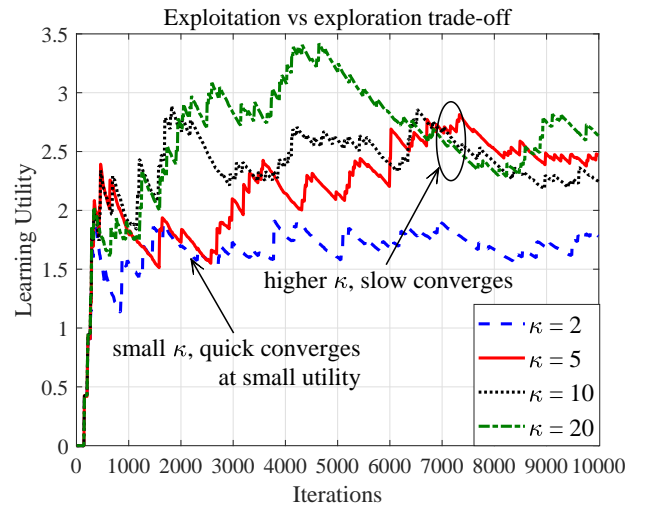


Fig. 7. Convergence of the proposed learning algorithm.

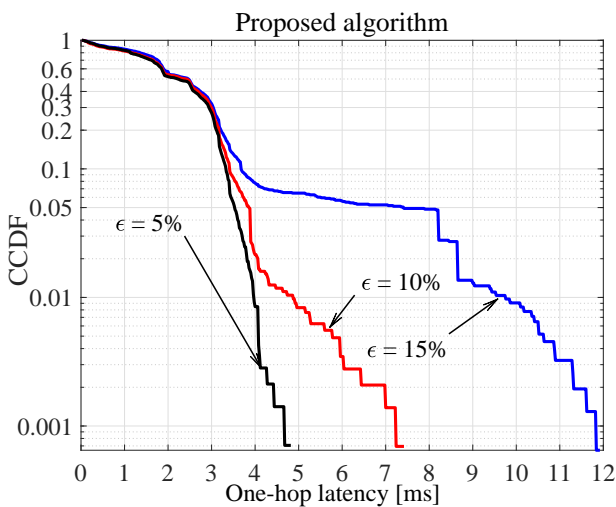


Fig. 6. CCDF of one-hop latency versus the guaranteed probability ϵ , $\beta = 10$ ms, $\kappa = 5$, and $\bar{\mu} = 4.5$ Gbps.

In Fig. 6, we report the tail distribution of the one-hop latency (in logarithmic scale) versus the guaranteed probability ϵ . By varying ϵ from 0.05 to 0.15, the system is allowed to achieve a delay greater than the target latency with higher probability. As can be seen in Fig. 6, the probability that the system achieves a latency greater than 4 ms increases from less than 1 % to 8 % when increasing ϵ from 0.05 to 0.15. This indicates the trade-off between reliability and latency, if we loose the reliability requirement, latency is higher.

A. Convergence Characteristics

We plot the learning convergence of the path selection scheme, based on the reinforcement learning algorithm as shown in Fig. 7. In this work, we have applied the Boltzmann-Gibbs technique to capture the trade-off between exploration and exploitation as per (19). We run the simulations for

different values of $\kappa \in \{2, 5, 10, 20\}$ for all flow f . As expected, with a small value of κ , the MBS decides to use the paths with highest payoff, selected at the beginning (a small probability of exploration). In this case, the algorithm converges faster, but lacks exploration, the MBS will not try other paths, which may exploit path diversity; as shown in Fig. 9, small value of κ , results in higher delay in the long run. By increasing κ , the MBS exploits the network environment with higher probability. The benefits of exploration are to utilize the path diversity, improving the performance, i.e., low latency and reducing congestion at the BSs. As shown in Fig. 9, average of latency is decreased with κ , and a large value of κ incurs slow convergence.

Next, we plot the convergence of the iterative algorithm as a function of the number of hops as shown in Fig. 8. Here, we provide the distribution of the number of iterations of the SOCP-based algorithm in which the convergence criteria stops running with an accuracy of 10^{-2} . With increasing the number of hops, the number of constraints and variables is increased, and thus the number of iterations required by the algorithm for convergence is higher. Intuitively, our proposed algorithm only needs few iteration to converge at each time slot t as shown in Fig. 8. For example, for three hop transmission, the probability that the number of iterations takes a value less than or equal to 7 is 90%.

B. Impact of the Learning Temperature

In addition to the previous discussion on the impact of the trade-off parameter on the convergence, in Fig. 9, we report the average one-hop latency versus the learning trade-off parameter, κ . It can be observed that at small κ , slowly increasing κ the MBS is allowed to explore other paths to get higher gain in the long run. Hence, the average one-hop latency gradually reduces with small increased κ . However, when κ is very large, four paths are determined uniformly for two flows, which becomes random path selection. For instance, when $\kappa = 50$, the average delay is much higher. Hence, it can

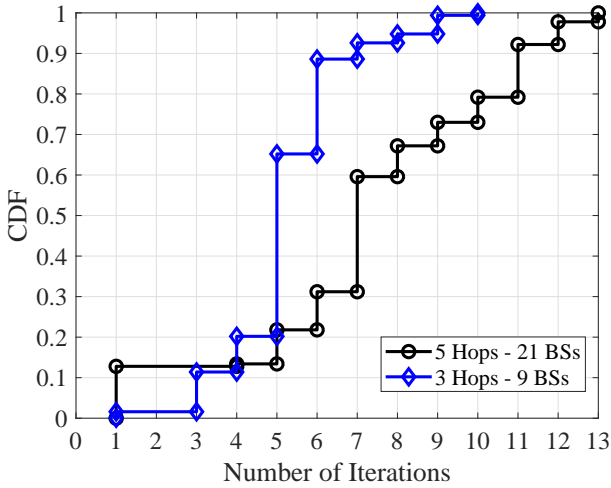


Fig. 8. The iterative algorithm convergence.

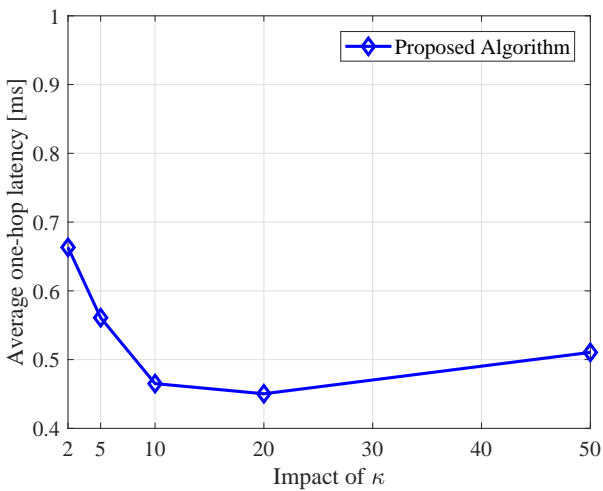


Fig. 9. Average one-hop delay versus the temperature parameter κ , $\epsilon = 0.05$, $\beta = 10$ ms, and $\bar{\mu} = 3.5$ Gbps.

be observed that the average delay is a convex function of κ in which there exists an optimal value for κ .

VII. CONCLUSION

In this paper, we proposed a multi-hop multi-path scheduling to support reliable communication by incorporating the probabilistic latency constraint and traffic splitting techniques in 5G mmWave networks. In particular, the problem is modeled as a network utility maximization subject to a bounded latency with a guaranteed reliability probability, and network stability. We employed massive MIMO and mmWave communication techniques to further improve the DL transmission of a multi-hop self-backhauled small cells. By leveraging stochastic optimization, the problem is decoupled into path selection and rate allocation, which are solved by applying the reinforcement learning and successive convex approximation methods,

respectively. A comprehensive performance analysis of our proposed algorithm is mathematically provided. Numerical results show that our proposed framework reduces latency by 50.64% and 92.9% as compared to the *baselines* with and without learning, respectively.

ACKNOWLEDGMENT

The authors would like to acknowledge colleagues Chen-Feng Liu, Mohammed Elbamby, Kien Giang Nguyen, Satya Joshi, Quang-Doanh Vu, Sumudu Samarakoon, and Jihong Park at CWC, University of Oulu for helpful discussions on the paper.

REFERENCES

- [1] T. K. Vu, C.-F. Liu, M. Bennis, M. Debbah, and M. Latva-aho, "Path Selection and Rate Allocation in Self-Backhauled mmWave Networks," in *Proc. IEEE Wireless Communications and Networking Conference (WCNC)*, Barcelona, Catalonia, Spain, Apr. 2018.
- [2] J. G. Andrews et al., "What Will 5G Be?" *IEEE Journal on Selected Areas in Communications*, vol. 32, no. 6, pp. 1065–1082, June 2014.
- [3] T. S. Rappaport et al., "Millimeter wave mobile communications for 5G cellular: It will work!" *IEEE Access*, vol. 1, pp. 335–349, 2013.
- [4] F. Gómez-Cuba, E. Erkip, S. Rangan, and F. J. González-Castaño, "Capacity Scaling of Cellular Networks: Impact of Bandwidth, Infrastructure Density and Number of Antennas," *IEEE Transactions on Wireless Communications*, vol. 17, no. 1, pp. 652–666, 2018.
- [5] A. Anpalagan, M. Bennis, and R. Vannithamby, *Design and Deployment of Small Cell Networks*. Cambridge University Press, 2015.
- [6] T. K. Vu, M. Bennis, S. Samarakoon, M. Debbah, and M. Latva-aho, "Joint Load Balancing and Interference Mitigation in 5G Heterogeneous Networks," *IEEE Transactions on Wireless Communications*, vol. 16, no. 9, pp. 6032–6046, Sep. 2017.
- [7] E. Björnson, E. G. Larsson, and T. L. Marzetta, "Massive MIMO: Ten myths and one critical question," *IEEE Communications Magazine*, vol. 54, no. 2, pp. 114–123, 2016.
- [8] N. Bhushan et al., "Network densification: the dominant theme for wireless evolution into 5G," *IEEE Communications Magazine*, vol. 52, no. 2, pp. 82–89, 2014.
- [9] T. K. Vu, K. Sungoh, and O. Sangchul, "Cooperative Interference Mitigation Algorithm in Heterogeneous Networks," *IEICE Transactions on Communications*, vol. 98, no. 11, pp. 2238–2247, 2015.
- [10] T. K. Vu, C.-F. Liu, M. Bennis, M. Debbah, M. Latva-aho, and C. S. Hong, "Ultra-Reliable and Low Latency Communication in mmWave-Enabled Massive MIMO Networks," *IEEE Communications Letters*, vol. 21, no. 9, pp. 2041–2044, Sep. 2017.
- [11] M. Bennis, M. Debbah, and H. V. Poor, "Ultra-Reliable and Low-Latency Wireless Communication: Tail, Risk and Scale," *CoRR*, vol. abs/1801.01270, 2018. [Online]. Available: <http://arxiv.org/abs/1801.01270>
- [12] T. K. Vu, M. Bennis, M. Debbah, M. Latva-aho, and C. S. Hong, "Ultra-Reliable Communication in 5G mmWave Networks: A Risk-Sensitive Approach," *IEEE Communications Letters*, vol. 22, no. 4, pp. 708–711, 2018.
- [13] L. Schnack, C. Wolfe, and D. Olps, "In-band wireless communication network backhaul," Jan. 22 2008, US Patent 7,321,571.
- [14] O. Semiari, W. Saad, Z. Daw, and M. Bennis, "Matching theory for backhaul management in small cell networks with mmWave capabilities," in *Proc. IEEE International Conference on Communications (ICC)*. IEEE, 2015, pp. 3460–3465.
- [15] S. Hur et al., "Millimeter wave beamforming for wireless backhaul and access in small cell networks," *IEEE Trans. Commun.*, vol. 61, no. 10, pp. 4391–4403, Oct. 2013.

- [16] Qualcomm Technologies, Inc, "Leading the path towards 5G with LTE Advanced Pro," White Paper, 2016.
- [17] S. Singh, F. Ziliotto, U. Madhow, E. Belding, and M. Rodwell, "Blockage and directivity in 60 GHz wireless personal area networks: From cross-layer model to multihop MAC design," *IEEE Journal on Selected Areas in Communications*, vol. 27, no. 8, 2009.
- [18] N. Eshraghi, B. Maham, and V. Shah-Mansouri, "Millimeter-wave device-to-device multi-hop routing for multimedia applications," in *Proc. IEEE Int. Conf. Commun.*, Kuala Lumpur, Malaysia, May 2016, pp. 1–6.
- [19] A. Zhou, M. Liu, Z. Li, and E. Dutkiewicz, "Cross-layer design for proportional delay differentiation and network utility maximization in multi-hop wireless networks," *IEEE Transactions on Wireless Communications*, vol. 11, no. 4, pp. 1446–1455, 2012.
- [20] —, "Joint traffic splitting, rate control, routing, and scheduling algorithm for maximizing network utility in wireless mesh networks," *IEEE Transactions on Vehicular Technology*, vol. 65, no. 4, pp. 2688–2702, 2016.
- [21] B. Sahoo, C.-H. Yao, and H.-Y. Wei, "Millimeter-Wave Multi-Hop Wireless Backhauling for 5G Cellular Networks," in *Proc. IEEE 85th Vehicular Technology Conf.*, Sydney, Australia, June 2017, pp. 1–6.
- [22] P. Key et al., "Path selection and multipath congestion control," in *Proc. the 26th IEEE Int. Conf. on Computer Communications (INFOCOM)*. Barcelona, Spain: IEEE, 2007, pp. 143–151.
- [23] N. Yong et al., "A survey of millimeter wave communications (mmWave) for 5G: opportunities and challenges," *Wireless Networks*, vol. 21, no. 8, pp. 2657–2676, 2015.
- [24] M. J. Neely, "Stochastic network optimization with application to communication and queueing systems," *Synthesis Lectures on Communication Networks*, vol. 3, no. 1, pp. 1–211, 2010.
- [25] J. García-Rois, F. Gómez-Cuba, M. R. Akdeniz, F. J. González-Castaño, J. C. Burguillo, S. Rangan, and B. Lorenzo, "On the analysis of scheduling in dynamic duplex multihop mmwave cellular systems," *IEEE Transactions on Wireless Communications*, vol. 14, no. 11, pp. 6028–6042, 2015.
- [26] L. X. Bui, R. Srikant, and A. Stolyar, "A novel architecture for reduction of delay and queueing structure complexity in the backpressure algorithm," *IEEE/ACM Transactions on Networking (TON)*, vol. 19, no. 6, pp. 1597–1609, 2011.
- [27] E. Stai and S. Papavassiliou, "User optimal throughput-delay trade-off in multihop networks under num framework," *IEEE Communications Letters*, vol. 18, no. 11, pp. 1999–2002, 2014.
- [28] H. Q. Ngo, E. G. Larsson, and T. L. Marzetta, "Energy and spectral efficiency of very large multiuser MIMO systems," *IEEE Transactions on Communications*, vol. 61, no. 4, pp. 1436–1449, 2013.
- [29] S. Samarakoon, M. Bennis, W. Saad, and M. Latva-aho, "Backhaul-aware interference management in the uplink of wireless small cell networks," *IEEE Transactions on Wireless Communications*, vol. 12, no. 11, pp. 5813–5825, 2013.
- [30] G. Yang, M. Haenggi, and M. Xiao, "Traffic allocation for low-latency multi-hop millimeter-wave networks with buffers," *submitted to IEEE Transactions on Communications*, 2017.
- [31] T. K. Vu, M. Bennis, S. Samarakoon, M. Debbah, and M. Latva-aho, "Joint in-band backhauling and interference mitigation in 5G heterogeneous networks," in *Proc. 22th European Wireless Conf.*, Oulu, Finland, May 2016, pp. 1–6.
- [32] Z. Zhang, X. Chai, K. Long, A. V. Vasilakos, and L. Hanzo, "Full duplex techniques for 5G networks: self-interference cancellation, protocol design, and relay selection," *IEEE Communications Magazine*, vol. 53, no. 5, pp. 128–137, 2015.
- [33] A. Zakrzewska et al., "Dual connectivity in LTE HetNets with split control-and user-plane," in *Proc. IEEE Global Commun. Conf. Workshops*, Atlanta, GA, USA, Dec. 2013, pp. 391–396.
- [34] J. Liu and E. S. Bentley, "Hybrid-Beamforming-Based Millimeter-Wave Cellular Network Optimization," in *Proc. 15th International Symposium on Modeling and Optimization in Mobile, Ad Hoc, and Wireless Networks (WiOpt)*, 2017, pp. 1–8.
- [35] J. Wildman et al., "On the joint impact of beamwidth and orientation error on throughput in directional wireless Poisson networks," *IEEE Transactions on Wireless Communications*, vol. 13, no. 12, pp. 7072–7085, 2014.
- [36] C. Perfecto, J. Del Ser, and M. Bennis, "Millimeter-wave v2v communications: Distributed association and beam alignment," *IEEE Journal on Selected Areas in Communications*, vol. 35, no. 9, pp. 2148–2162, 2017.
- [37] T. L. Marzetta and B. M. Hochwald, "Fast transfer of channel state information in wireless systems," *IEEE Transactions on Signal Processing*, vol. 54, no. 4, pp. 1268–1278, 2006.
- [38] J. Palacios et al., "Tracking mm-Wave Channel Dynamics: Fast Beam Training Strategies under Mobility," in *Proc. 36th Annual IEEE Int. Conf. on Computer Communications (INFOCOM)*, Atlanta, GA, USA, 2017, pp. 1–9.
- [39] J. D. Little and S. C. Graves, "Little's law," in *Building intuition*. Springer, 2008, pp. 81–100.
- [40] M. S. Elbambay, C. Perfecto, M. Bennis, and K. Doppler, "Toward low-latency and ultra-reliable virtual reality," *IEEE Network*, vol. 32, no. 2, pp. 78–84, 2018.
- [41] A. Mukherjee, "Queue-aware dynamic on/off switching of small cells in dense heterogeneous networks," in *Proc. IEEE Global Commun. Conf. Workshops*, Atlanta, GA, USA, Dec. 2013, pp. 182–187.
- [42] L. Huang, "Receding learning-aided control in stochastic networks," *Perform. Eval.*, vol. 91, no. C, pp. 150–169, Sep. 2015.
- [43] M. Bennis, S. M. Perlaza, P. Blasco, Z. Han, and H. V. Poor, "Self-organization in small cell networks: A reinforcement learning approach," *IEEE transactions on wireless communications*, vol. 12, no. 7, pp. 3202–3212, 2013.
- [44] S. M. Perlaza, H. Tembine, S. Lasaulce, and M. Debbah, "Quality-of-service provisioning in decentralized networks: A satisfaction equilibrium approach," *IEEE Journal of Selected Topics in Signal Processing*, vol. 6, no. 2, pp. 104–116, 2012.
- [45] S. Boyd and L. Vandenberghe, *Convex optimization*. Cambridge university press, 2004.
- [46] K.-G. Nguyen, L.-N. Tran, O. Tervo, Q.-D. Vu, and M. Juntti, "Achieving energy efficiency fairness in multicell MISO downlink," *IEEE Commun. Lett.*, vol. 19, no. 8, pp. 1426–1429, Aug. 2015.
- [47] A. Ben-Tal and A. Nemirovski, *Lectures on modern convex optimization: analysis, algorithms, and engineering applications*. SIAM, 2001.
- [48] A. Beck, A. Ben-Tal, and L. Tretushvili, "A sequential parametric convex approximation method with applications to nonconvex truss topology design problems," *Journal of Global Optimization*, vol. 47, no. 1, pp. 29–51, 2010.
- [49] M. R. Akdeniz, Y. Liu, M. K. Samimi, S. Sun, S. Rangan, T. S. Rappaport, and E. Erkip, "Millimeter wave channel modeling and cellular capacity evaluation," *IEEE J. Sel. Areas Commun.*, vol. 32, no. 6, pp. 1164–1179, Jun. 2014.
- [50] T. K. Vu, M. Bennis, M. Debbah, and M. Latva-aho, "Matlab Code for the Joint Path Selection and Rate Allocation Framework for 5G Self-Backhauled mmWave Networks," <https://github.com/TrungKienVu069>, 2018.
- [51] M. Weiner et al., "Design of a low-latency, high-reliability wireless communication system for control applications," in *Proc. IEEE Int. Conf. Commun.*, Sydney, NSW, Australia, Jun. 2014, pp. 3829–3835.